



Saldivia, M. et al. (2020) Targeting the trypanosome kinetochore with CLK1 protein kinase inhibitors. *Nature Microbiology*, 5(10), pp. 1207-1216.

There may be differences between this version and the published version. You are advised to consult the publisher's version if you wish to cite from it.

<https://eprints.gla.ac.uk/224292/>

Deposited on: 20 January 2022

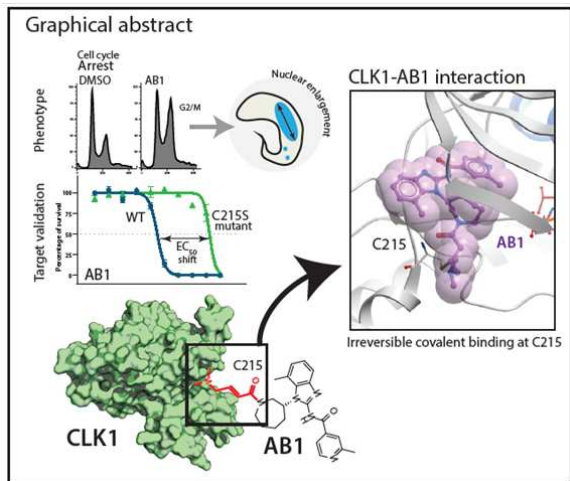
Enlighten – Research publications by members of the University of Glasgow
<https://eprints.gla.ac.uk>

1 Targeting the trypanosome kinetochore with CLK1 protein 2 kinase inhibitors

3
4 Manuel Saldivia¹, Eric Fang², Xiaolei Ma², Elmarie Myburgh³, Juliana B. T. Carnielli¹, Christopher
5 Bower-Lepts¹, Elaine Brown¹, Ryan Ritchie⁴, Suresh B. Lakshminarayana⁵, Yen-Liang Chen⁵,
6 Debjani Patra⁵, Elizabeth Ornelas², Hazel X. Y. Koh⁵, Sarah Williams², Frantisek Supek⁶, Daniel
7 Paape⁴, Richard McCulloch⁴, Marcel Kaiser^{7,8}, Michael P. Barrett⁴, Jan Jiricek⁵, Thierry T. Diagana⁵,
8 Jeremy C. Mottram^{1*} and Srinivasa P.S. Rao^{5*}

9 ¹York Biomedical Research Institute, Department of Biology, University of York, UK. ²Novartis Institutes for Biomedical
10 Research, USA. ³York Biomedical Research Institute, Hull York Medical School, University of York, UK. ⁴Institute of
11 Infection, Immunity and Inflammation, University of Glasgow, UK. ⁵Novartis Institute for Tropical Diseases, USA.
12 ⁶Genomics Institute of the Novartis Research Foundation, USA. ⁷Swiss Tropical and Public Health Institute, Switzerland.
13 ⁸University of Basel, Switzerland.

14
15 * Corresponding authors: jeremy.mottram@york.ac.uk; srinivasa.rao@novartis.com



16 17 18 **ABSTRACT**

19 **The kinetochore is a macromolecular structure that assembles on the centromeres of**
20 **chromosomes and provides the major attachment point for spindle microtubules during**
21 **mitosis. In *Trypanosoma brucei* the proteins that make up the kinetochore are highly**
22 **divergent, with the inner kinetochore comprising at least 20 distinct and essential**

23 **proteins (KKT1-20) that include four protein kinases, CLK1 (KKT10), CLK2 (KKT19),**
24 **KKT2 and KKT3. We report the identification and characterisation of the**
25 **amidobenzimidazoles (AB) protein kinase inhibitors that have nanomolar potency**
26 **against *T. brucei* bloodstream forms, *Leishmania* and *Trypanosoma cruzi*. Target**
27 **deconvolution using a selection of 31 *T. brucei* mutants that over-express known**
28 **essential protein kinases identified CLK1 as a primary target. Biochemical studies and**
29 **the co-crystal structure of CLK1 in complex with AB1 show that the irreversible**
30 **competitive inhibition of CLK1 is dependent on a Michael acceptor forming an**
31 **irreversible bond with C215 in the ATP binding pocket, a residue that is not present in**
32 **human CLK1, thereby providing selectivity. Chemical inhibition of CLK1 impairs**
33 **inner kinetochore recruitment and compromises cell cycle progression, leading to cell**
34 **death. This work highlights a unique drug target for trypanosomatid parasitic protozoa**
35 **and a new chemical tool for investigating the function of their divergent kinetochores.**

36

37 **Main Text**

38 The three kinetoplastid neglected tropical diseases; leishmaniasis, Chagas disease, and human
39 African trypanosomiasis (HAT) remain a significant global health burden. Over a billion
40 people living in endemic regions are at risk from these neglected diseases with an estimated
41 30,000 deaths annually (WHO)¹. While there have been notable recent advances in disease
42 control, current therapies have severe shortcomings and there is an urgent need for innovative
43 treatments that are safe, efficacious and easy to administer. Some of the significant advances
44 include the development of novel oral therapy for sleeping sickness^{2,3} and identification of
45 pre-clinical candidates for leishmaniasis⁴⁻⁶. In order to find additional growth inhibitors, a
46 whole parasite based phenotypic screen was carried out using ~2.3 million compounds
47 against bloodstream forms of *T. brucei*⁴, which included the Novartis kinase focused inhibitor
48 library. This led to the identification of AB0, an Amidobenzimidazole (Fig. 1a and
49 Supplementary Figure 1a) with an EC₅₀ of 290 nM in an *in vitro* *T. brucei* parasite growth
50 inhibition assay (Fig. 1a).

51 Detailed structure activity relationship (SAR) studies using ~250 close analogs obtained from
52 the Novartis compound archive and focused medicinal chemistry efforts were carried out.
53 The growth inhibition activity of compounds against *T. brucei* ranged 3 log orders with many
54 compounds showing < 100 nM potency. Results also showed that the analogs having Michael

55 acceptor chemical functionality are critical for potent activity and afford higher lipophilic
56 efficiency (LipE >3) required for more favourable drug-like properties (Fig. 1b,
57 Supplementary Table 1). SAR analysis also led to the identification of more potent bioactive
58 compounds, including AB1 (EC₅₀ of 72 nM against *T. brucei*), with a >100-fold cytotoxicity
59 window (Fig. 1a). AB1 not only showed potent activity against *T. b. gambiense* and *T. b.*
60 *rhodesiense*, the causative agents of sleeping sickness but also had pan-kinetoplastid activity
61 against *T. cruzi* (aetiology for Chagas disease), *Leishmania mexicana* (cutaneous
62 leishmaniasis) and *L. donovani* (visceral leishmaniasis) suggesting that the molecular target is
63 conserved across trypanosomatids (Fig. 1a). Compound AB1 was cidal to *T. brucei* showing
64 concentration and time dependent kill, further it also exhibited relapse free cidal activity in wash-
65 off assays suggesting ability to achieve sterile cure (Extended data 1b, c). In vitro wash-off
66 assays are presumed to be predictive of compounds' ability to achieve relapse free cure in the
67 mouse model of infection. AB1 had better solubility and *in vitro* pharmacokinetic properties
68 with moderate to low clearance in mice, rat and human microsomes (Fig. 1a), allowing us to
69 evaluate the ability to cure *T. brucei* infection in mouse models.

70 *In vivo* efficacy of AB1 was tested in mice with haemolymphatic and central nervous system
71 (CNS) *T. brucei* infections using both STIB795 and GVR35 optimised bioluminescence HAT
72 mouse models⁷. A dose dependent cure was observed with AB1, resulting in relapse free cure
73 with a daily oral dosage of 50 mg/kg for four consecutive days in the STIB795
74 haemolymphatic mouse model of infection (Fig. 1c). However, despite a 4 log reduction in
75 parasitaemia observed in a pleomorphic GVR35 strain chronic (CNS) model of infection, the
76 parasitemia relapsed, most likely due to poor access of AB1 to parasites in the brain
77 (Extended data 2a,b). Although AB1 showed good brain partitioning (measured brain to
78 plasma ratio was 0.5), due to high brain tissue binding (>99%), the free fraction available for
79 acting against the parasites in the brain was negligible, leading to poor efficacy (Extended
80 data 2c,d). Further medicinal chemistry optimization is required to find compounds with
81 better pharmacokinetic properties in order to achieve cure in the CNS model. The mouse
82 efficacy studies using AB1 showed *in vivo* chemical validation of AB series compounds as
83 promising anti-trypanosomatid candidates.

84 AB1 is a known covalent inhibitor of mutant human epidermal growth factor receptor
85 (hEGFR) kinase, a well-studied target for non-small cell lung cancer (Fig 1a)⁸. Whilst
86 hEGFR belongs to the tyrosine kinase family, the *T. brucei* genome lacks members of the
87 receptor-linked or cytosolic tyrosine kinase families⁹. A major challenge for phenotypic hits

88 is to identify the molecular target that is responsible for that effect. Since AB series
89 compounds were hypothesized to target protein kinases, we generated inducible *T. brucei*
90 gain-of function mutants of individual protein kinases to screen for resistance to AB1 (Fig.
91 2a). Twenty-nine essential protein kinases that had been assessed previously by RNAi as
92 having specific RNAi induced cell cycle defects in bloodstream forms (BSF)¹⁰ were
93 analysed. In our screen, only one protein kinase, CLK1, showed a significant 6.5-fold
94 increase in resistance compared with its uninduced control (Fig. 2b). In general over-
95 expression of protein kinases show moderate resistance to their inhibitors. Wyllie and co-
96 workers showed that co-over expression of CYC9 and wild type CRK12 in *L. donovani*
97 resulted in 3-fold shift in cellular EC₅₀ against the compound **5** (DDD853651/GSK3186899),
98 validating CRK12 as the target⁵. Over-expression of PI4K (phosphatidylinositol 4-kinase) in
99 *Plasmodium falciparum* also rendered moderate 3-fold shift in EC₅₀ against imidazopyrazine
100 compounds, confirming the on-target effect¹¹.

101 In mammals, CLK1 belongs to the Clk (Cdc2-like kinase) family implicated in RNA splicing
102 control and consists of at least four members¹². In *T. brucei*, CLK1 is a kinetochore
103 component essential for mitosis and has been proposed to be one of the potential targets for
104 the fungal antibiotic hypothemycin¹³⁻¹⁵. As treatment with AB1 resulted in a G2/M cell cycle
105 arrest (Fig. 2c-e) with most of the treated cells having an enlarged nucleus (Fig. 2d) similar to
106 CLK1 RNAi knockdown (Extended data 3a-c), we tested if overexpression of CLK1 would
107 confer resistance to drug-induced G2/M cell cycle arrest. Indeed, parasites overexpressing
108 CLK1 had a normal cell cycle profile after treatment with AB1, in comparison to the parental
109 cell line and DMSO uninduced control, which were G2/M arrested after treatment (Fig. 2c).
110 CLK1 overexpression impairs parasite fitness without affecting cell cycle progression,
111 suggesting that *T. brucei* tightly regulates CLK1 expression (Extended data 3d). In addition,
112 AB1 attenuates CLK1 toxicity caused by over-expression, providing further evidence that
113 CLK1 is the compound's primary target (Extended data 3e, f).

114 We expressed recombinant TbCLK1 and human CLK1 and tested ~230 compounds from the
115 AB series to determine the biochemical SAR. Apparent IC₅₀ was determined after 10 min
116 post-incubation with the enzyme. A strong correlation was observed between inhibition of the
117 *T. brucei* CLK1 enzyme and cellular activity (Pearson's correlation $r = 0.68$), supporting the
118 chemical validation of CLK1 as the molecular target for the amidobenzimidazole series of
119 compounds (Fig. 3a, Supplementary Table 1). The majority of the compounds showed greater
120 selectivity against TbCLK1 compared to hCLK1 (Fig. 3b, Supplementary Table 1). AB1

121 inhibited TbCLK1 with an apparent IC_{50} of 10 nM, with 90-fold selectivity observed over
122 hCLK1 (Fig. 3b). *T. brucei* also has another protein kinase, CLK2, which is closely related to
123 CLK1, with 92% overall sequence identity and 100% identity in the protein kinase domain.
124 CLK2 is less abundant than CLK1 in bloodstream forms (Extended data 4a, b). AB1 would
125 be expected to inhibit the kinase activity of CLK2, but this is unlikely to contribute to killing
126 in bloodstream forms of the parasite as CLK2-specific RNAi suggests the protein is not
127 essential¹³.

128 Interestingly, all compounds with a Michael acceptor inhibited TbCLK1 kinase activity but
129 not others, strongly suggesting this functionality is an essential feature of the pharmacophore
130 (Fig. 3a). In order to test the putative critical role played by the Michael acceptor, a
131 compound similar to AB1, which has a saturated double bond at the Michael acceptor, was
132 profiled in both enzymatic and cellular assays. This compound (AB2) was completely
133 inactive in both TbCLK1 enzyme (apparent $IC_{50} > 20 \mu M$) and whole cell growth inhibition
134 assays (Tbb $EC_{50} > 50 \mu M$), confirming the importance of the Michael acceptor for activity
135 (Supplementary Table 1). The hEGFR inhibitors having Michael acceptors are known to
136 covalently interact with an active site cysteine (C797) near the ATP binding domain^{8,16}.

137 In order to directly visualize the binding mode, structure of TbCLK1 kinase domain bound to
138 AB1 was determined to 2.7Å (PDB 6Q2A) (Fig. 3c). At this resolution, the electron density
139 map has continuous density between the side-chain of the thiol group of C215 and the
140 Michael acceptor of the inhibitor (Fig. 3c, d), strongly indicating the formation of an
141 irreversible covalent bond between them. Furthermore, AB1 forms direct hydrogen bonds
142 with the backbone amide NH of Y212 and C215 and a salt bridge with D218 (Fig. 3c),
143 consistent with the binding mode of AB1 when covalently attached to hEGFR⁸. While both
144 hEGFR and TbCLK1 have cysteine in their active sites, hCLK1 lacks cysteine and instead
145 has serine in the same position (Extended data 5a-c). This has led to achieving significant
146 selectivity for most AB series compounds for TbCLK1 (Fig. 3b). Beyond the AB1 binding
147 site, the TbCLK1 kinase domain exhibits an overall structure that is in line with a kinase in
148 the active conformation, closed kinase lobes, a well-ordered activation loop, DLG-in and an
149 intact salt bridge to αC -helix (Fig. 3c).

150 To investigate the covalent binding and interaction with C215, we co-incubated AB1 and
151 AB2 with both wild type and C215A mutant of TbCLK1 and assessed the interaction using
152 biophysical methods. As expected, incubation of AB1 with wild type TbCLK1 enzyme

153 resulted in a 12° C shift in denaturing temperature as seen by differential scanning
154 fluorimetry (Fig. 4a and Extended data 6a). Similarly, mass spectrometric analysis also
155 showed one main product per protein which has an average mass 475 Da higher than the
156 unmodified protein (Extended data 6b). This was consistent with the addition of one molecule
157 of AB1, which has a mass of 475 Da. No shift in the mass was seen for AB2, or in C215A
158 mutant CLK1 (Extended data 6a). These results clearly show covalent interaction of the
159 Michael acceptor with C215 of TbCLK1. In addition, TbCLK1 C215A is not inhibited by
160 AB1, but is inhibited by the non-covalent pan-kinase inhibitor staurosporine (Fig. 4b).
161 Multiple sequence alignment of CLK1 from *T. brucei*, *T. cruzi* and *L. mexicana* showed high
162 sequence similarity and C215 was conserved across parasites, further suggesting the growth
163 inhibition of these parasites by AB1 could be due to TbCLK1 inhibition (Extended data 4c).

164 Further, to assess the importance of *T. brucei* CLK1 C215 in AB1 binding in parasites, a
165 recoded version of CLK1 that contained a Cys to Ala mutation at position 215 was expressed
166 in the TbCLK1 RNAi line. In this cell line, RNAi induction depleted the wild type CLK1
167 mRNA but the recoded CLK1 C215A mRNA was not susceptible to RNAi-induced
168 degradation and was expressed. This triggered a G2/M cell cycle arrest, suggesting this
169 residue is important for CLK1 function and may mimic AB1 –TbCLK1 mediated inhibition.
170 Since expression of the C215A mutation affected the fitness of the parasites, we attempted to
171 express a C215S mutation, as human CLK1 has serine at position 215. Parasites expressing
172 the TbCLK1 C215S mutation had a normal cell cycle profile (Extended data 7a, b) and were
173 resistant to treatment with 5x EC₅₀ of AB1 (Extended data 7c). Thus, we evaluated if the
174 overexpression of the C215S mutation in the parental cell line increased this resistance, and
175 indeed, this mutation conferred a > 60-fold EC₅₀ shift of resistance against AB1 (Fig. 4c),
176 which also significantly reduced the effect of AB1 in the parasite's growth and survival (Fig.
177 4d, e). Interestingly, we observed that AB1 treatment induced a mobility shift on CLK1,
178 which likely corresponds to phosphorylation, whilst the C215S mutant protein remained
179 unaltered (Extended data 7d). Together, these data demonstrate target engagement in the
180 parasite and inhibition of CLK1 with AB1.

181 TbCLK1 (KKT10) is a core component of the inner kinetochore. In other organisms, the
182 kinetochore supports directional movement of chromosomes into microtubules to ensure
183 faithful chromosome segregation¹⁷. Some of the *T. brucei* kinetochore components have been
184 recently described, and grouped according to their patterns of expression/localization through
185 the cell cycle^{14,18}. The significant divergence between components of the human and parasite

186 kinetochores underpins its potential druggability. Although depletion of TbCLK1 has been
187 associated with the presence of lagging chromosomes during mitosis in procyclic cells¹⁴ the
188 causal link of TbCLK1 to this process has yet to be established. To investigate this further *T.*
189 *brucei* bloodstream form cells were synchronised by cell sorting¹⁹ to give 2C and 4C nuclear
190 DNA content populations and then allowed to enter the cell cycle in the presence or absence
191 of AB1 (Fig 2e and Extended data 8 a-c). Inhibition of TbCLK1 in the 2C population (G1-
192 phase) synchronously progressing through the cell cycle led to arrest of cells in late
193 metaphase with a 2K1N configuration (defined as cells having 2 kinetoplasts (2K) and 1
194 nucleus (1N)). By contrast, inhibition of TbCLK1 in the 4C population synchronously
195 progressing through the cell cycle induced an arrest in the late anaphase (2K2N population).
196 These data are consistent with inhibition of TbCLK1 causing a disruption in kinetochore
197 function during metaphase and exit from anaphase into cytokinesis. To confirm this, we
198 tagged KKT2, a canonical centromere kinetochore protein, with mNeonGreen and assessed
199 its localisation in the presence and absence of AB1. Similar to previous observations in
200 procyclic form cells^{14,18}, we observed in bloodstream form cells that KKT2 is constitutively
201 expressed until anaphase. Treatment with either 2 x EC₅₀ of AB1 for 24 hr or 5 x EC₅₀ of
202 AB1 for 6 hr caused dispersal of the defined foci of the kinetochore within the nucleus (Fig.
203 5a). This change of KKT2 pattern was also observed after depletion of CLK1 by RNAi (Fig.
204 5b). These data demonstrate that inhibition of CLK1 by AB1 causes impairment of
205 kinetochore function thereby defining a consequence of AB1 treatment.

206 **Discussion**

207 Our studies indicate that the principal mechanism of action for the amidobenzimidazole series
208 is inhibition of the trypanosome CLK1 protein kinase. In support of this, we show for over
209 230 compounds that a strong correlation exists between inhibition of recombinant TbCLK1
210 and killing of the parasite. Only those compounds that have a Michael acceptor and are
211 predicted to form a covalent bond with C215 of CLK1 are active and the X-ray structure,
212 differential scanning fluorimetry and mass spectrum chromatograms clearly demonstrate the
213 covalent linkage for AB1. We also show that over-expression of CLK1 or the CLK1 C215S
214 mutant provide 6.5-fold or >60-fold resistance of the parasite to AB1, respectively,
215 demonstrating target engagement. AB1 treatment of bloodstream form trypanosomes lead to
216 chromosome mis-segregation and cell cycle arrest, consistent with inhibition of CLK1, which
217 is a kinetochore kinase (KKT10). Generation of parasites resistant to compounds and the
218 identification of mutations in target genes is a well-established method for target

219 deconvolution^{4,5}. However, we failed to generate parasites resistant to AB1, even after a year
220 and half under compound selection. This might be explained if AB1 has an element of
221 polypharmacology and one potential secondary target is CLK2, which is an active enzyme²⁰
222 and has an identical protein kinase domain to CLK1, thus inhibited by AB1. In procyclic
223 form trypanosomes CLK1 and CLK2 are functionally redundant²¹, whilst in bloodstream
224 form parasites CLK1 is essential, but CLK2 is not essential^{15,22}. An explanation for this
225 arises from our finding that CLK1 is more highly expressed than CLK2 in bloodstream
226 forms, such that inhibition of CLK1 activity leads to chromosome mis-segregation and cell
227 cycle arrest, phenotypes consistent with inhibition of a kinetochore kinase (KKT10).

228

229 We propose that inhibition of CLK1 activity with AB1 leads to impaired kinetochore
230 function and irreversible arrest in metaphase leading to cell death. A combination of growth
231 inhibition screening, target identification and characterization resulted in the chemical
232 validation of CLK1 as a unique pan-kinetoplastid drug target. In recent years six covalent
233 inhibitors of protein kinases have been successfully approved for cancer treatment²³,
234 underlining the possibility of developing covalent inhibitors into drugs. The combination of a
235 distinct mechanism of action targeting the kinetochore, and a new series of
236 antitrypanosomatid AB compounds, which have reduced chances of acquiring resistance in
237 the clinic, add to the proteasome and CRK12 inhibitors already entering clinical trials^{4,5,24,25}.
238 One of the key challenges for the AB series of compounds to progress to the clinic is to
239 improve kinase selectivity and the co-crystal structure determined in the current study will
240 significantly help in structure based medicinal chemistry optimization to resolve this issue.
241 The current efforts of CLK1 target validation also open up opportunities for focused
242 structure-based drug design using fragment screens in order to obtain non-covalent inhibitors
243 that have pan-kinetoplastid growth inhibition properties. In addition, the high level of
244 sequence divergence of trypanosome kinetochore complex proteins from humans^{14,26} make
245 the kinetochore a high value target.

246

247 **Contributions**

248 J.C.M, T.T.D and S.P.S.R planned the studies. Compounds synthesis, compound docking,
249 PK assays, and library screening by H.X.Y.K, D.P, Y.L.C, S.B.L, S.W, F.S and J.J; HAT
250 animal studies by E.M, R.R, M.P.B and M.K; generation of individual protein kinase cell

251 lines by E.B and M.S; Compound target deconvolution, TbCLK1 functional
252 characterisation, immunofluorescences and data analysis were performed by M.S and
253 J.B.T.C.; protein recombinant production, kinase assays and mass spectrometry by E.F,
254 De.P, C.B-L and M.S; Crystallization and structure determination by E.O, X.M.;CLK1
255 mutants plasmids designed and prepared by M.S, Da.P and R.M; J.C.M, S.P.S.R, and M.S
256 prepared and wrote the manuscript. All authors reviewed, edited and approved the paper.
257 J.C.M, S.P.S.R, M.P.B and T.T.D obtained funding.

258

259 **Data availability**

260 All the source data used for generating Figures 1-5 and Extended Data Figures 1-8 have been
261 provided as source data. Any other data that support the findings of this study are available
262 from the corresponding author upon request. *Trypanosoma brucei* CLK1 kinase domain in
263 complex with covalent aminobenzimidazole inhibitor AB1 is annotated in PDB with an
264 accession number 6Q2A.

265 **Competing interests**

266 The authors declare no competing interests, except that some authors have shares in
267 Novartis.

268

269 **Corresponding author**

270 Correspondence to Jeremy Mottram and Srinivasa P.S. Rao.

271 **METHODS**

272

273 **Cellular assays**

274

275 A kinase focused inhibitor library (containing approximately 10,000 compounds) was
276 screened at a single concentration of 10 μ M for the ability of compounds to inhibit growth of
277 *T. b. brucei* Lister 427. This resulted in 2264 compounds showing > 50% growth inhibition.
278 Chemi-informatic analysis of hits resulted in ~200 clusters, representatives of these were
279 subjected to 10-point dose-response growth inhibition assays against bloodstream form of *T.*
280 *b. brucei* Lister 427. Further removal of non-favourable chemical structures such as

281 nitrofuranes, cytotoxicity profiling using the HepG2 cell line (selectivity index of 10) and
282 favourable physico-chemical properties (polar surface area <100; molecular weight <500 and
283 lipophilicity <4.5) led to identification of an amidobenzimidazole scaffold (AB0) for further
284 follow up.

285

286 Bloodstream form of *Trypanosoma brucei brucei* Lister 427, *T. b. gambiense* STIB930 and
287 *T. b. rhodesiense* STIB900 were cultured in HMI-9 medium as described elsewhere⁴.
288 Other kinetoplastid parasites *Leishmania donovani* HU3 and *L. mexicana*
289 (MNYC/BZ/62/M379) were cultured in RPMI 1640 media as described earlier^{4,27}. The *T.*
290 *cruzi* Tulahuen parasites constitutively expressing *Escherichia coli* β -galactosidase²⁸ were
291 maintained in tissue culture as an infection in NIH 3T3 fibroblast cells⁴. NIH 3T3 and
292 human epithelial (HepG2) cells were obtained from ATCC and grown in RPMI media
293 (Life Technologies).

294 All other transgenic *T. b. brucei* parasites used in this study were derived from
295 monomorphic *T. b. brucei* 2T1 bloodstream forms²⁹ and were cultured in HMI-11 [HMI-9
296 (GIBCO) containing 10% v/v foetal bovine serum (GIBCO), Pen/Strep solution (penicillin
297 20 U ml⁻¹, streptomycin 20 mg ml⁻¹)] at 37 °C/5% CO₂ in vented flasks. Selective
298 antibiotics were used as follows: 5 μ g ml⁻¹ blasticidin or hygromycin and 2.5 μ g
299 ml⁻¹ phleomycin or G418. RNAi or overexpression was induced *in vitro* with tetracycline
300 (Sigma Aldrich) in 70% ethanol at 1 μ g ml⁻¹. Endogenous Ty, mNeonGreen or myc-
301 overexpression tagging were performed using the pPOTv6 vector³⁰ and pRPa²⁹, respectively.
302 The generation of inducible TbCLK1 RNAi was generated as previously described¹³. All
303 primers are listed in Supplementary methods Table 1.

304

305 All cell based assays were performed as described before^{4,31}. Briefly, bloodstream form of *T.*
306 *b. brucei* Lister 427, *T. b. rhodesiense* and *T. b. gambiense* parasites were incubated with
307 varying concentration of compounds for 48 hr. Cell viability was assessed by measuring ATP
308 levels using CellTiter-Glo reagent (Promega) and 50% growth inhibition (EC₅₀) was
309 calculated using sigmoidal dose response curves. For both intracellular *T. cruzi* amastigotes
310 and *L. donovani* HU3 axenic amastigotes growth inhibition was measured as described
311 earlier⁴. Intracellular *L. mexicana* amastigote growth inhibition was assessed by microscopy.
312 Briefly, after primary peritoneal mouse macrophages were infected with late-log-phase
313 promastigotes at an infection ratio of 10:1; non-internalized parasites were removed by

314 washing the plates with PBS, and cells were cultured with different drug concentrations for
315 96 hr. Determination of intracellular parasite numbers were done by fixing the cells in
316 methanol and then stained with DAPI. Cytotoxicity (CC_{50}) was also measured against mouse
317 fibroblast NIH 3T3 and HepG2 cell lines by incubating compounds for 4 days⁴.

318 Single protein kinase overexpression lines (Supplementary methods table 1) were generated
319 by transfecting *T. brucei brucei* 2T1 cells with a tetracycline inducible overexpression
320 plasmid linearized with *AscI* restriction enzyme. Each overexpression construct contains the
321 open reading frame (ORF) of a single protein kinase in the plasmid pGL2220 (pRPa-
322 iMYCx)³². This plasmid integrates at the tagged rRNA spacer (single locus) of 2T1 *T. brucei*.

323 Protein kinase overexpression cell lines were adjusted to 2×10^5 cells ml^{-1} and induced for
324 18 hr by the addition of tetracycline to a final concentration of $1 \mu g ml^{-1}$ in 70% ethanol. To
325 establish the EC_{50} , the protein kinase overexpression cell lines and parental control 2T1 were
326 treated with two-fold increasing concentrations of compounds (with similar DMSO
327 increasing concentration as control). Cell viability was measured at 48 hr with a POLARstar
328 Omega plate reader spectrophotometer; the determination of cell viability was carried out by
329 the established colorimetric technique using Alamar Blue (0.49 mM resazurin in phosphate-
330 buffered saline (PBS)), in a 96-well plate format spectrophotometric assay which measures
331 the ability of living cells to reduce resazurin. We used pentadimine isethionate (Sigma
332 Aldrich) as a positive control. Fluorescence emission was detected using a CLARIOstar ®
333 reader (BMG LABTECH; excitation filter at 540 nm and emissions filter at 590 nm). Fitting
334 of dose-response curves and IC_{50}/EC_{50} determination were normalized as percentage of
335 inhibition based on controls. Hesperadin was obtained from ApexBio Technology.

336

337 **Mouse infection models for *T. brucei*.**

338 The *T. brucei* strain STIB795 acute mouse model mimics the first stage of African
339 trypanosomiasis³³. Six female NMRI mice were used per experimental group, divided into
340 two cages (A and B). Each mouse was inoculated by intraperitoneal injection with 10^4
341 bloodstream forms of STIB795, respectively. Heparinized blood from a donor mouse with
342 approximately $5 \times 10^6 ml^{-1}$ parasitaemia was suspended in phosphate saline glucose (PSG) to
343 obtain a trypanosome suspension of $1 \times 10^5 ml^{-1}$. Each mouse was injected with 0.25 ml.
344 Compounds were formulated in 0.5% Tween80 in 0.5% methylcellulose. Compound
345 treatment was initiated 3 days post-infection and administered orally on four consecutive

346 days in a volume of 0.1 ml/10 g. Three mice served as infected-untreated controls. They were
347 not injected with the vehicle alone since we have established in our labs that these vehicles do
348 not affect parasitaemia nor the mice. Blood samples were taken after the 4th treatment. From
349 the mice in cage A, -1 h, 2 h and 8 h after the 4th treatment, 20 uL of blood each were taken
350 from the tail vein and from mice in cage B 1 h, 4 h, and 24 h after the 4th treatment.
351 Parasitaemia was monitored microscopically by tail blood examination twice a week until 31
352 days post-infection. Mice were considered cured when there was no parasitaemia relapse
353 detected in the tail blood over the 30-day observation period. *In vivo* efficacy studies in mice
354 were conducted at the Swiss Tropical and Public Health Institute (Basel) (License number
355 2813) according to the rules and regulations for the protection of animal rights
356 ("Tierschutzverordnung") of the Swiss "Bundesamt für Veterinärwesen". They were
357 approved by the veterinary office of Canton Basel-Stadt, Switzerland.

358

359 **Plasmids**

360 Recoded *CLK1* was synthesised by Eurofins Genomics. The recoded CLK1 sequence
361 (*CLK1^R*) codes for the same amino acid sequence as *CLK1* but only shares 95.06% nucleotide
362 identity. All segments of identity between *CLK1* and *CLK1^R* are less than 20 base pairs
363 long. *CLK1^R* was inserted by Gibson assembly® (New England Biolabs) into the plasmid
364 pGL2492 using *XbaI* and *BamHI* restriction sites, generating pGL2832. This plasmid is
365 designed to constitutively express CLK1 from the tubulin locus, with the addition of a C-
366 terminal 6x HA tag. To express the cysteine 215 mutants, the cysteine 215 was changed to
367 serine or alanine by mutating pGL2832, carrying the coding sequence for *CLK1*, using site
368 directed mutagenic PCR (Primer sequences in Supplementary methods). Similarly, C215S
369 mutation was introduced into original CLK1 OE plasmid, to generate CLK1 C215S OE
370 (NITD001 plasmid) into the parental 2T1 cell line.

371

372 **Immunofluorescence, cell cycle analysis and cell sorting**

373 Cells treated for 6 hr with compounds or DMSO were centrifuged at 1400 g for 10 min
374 before washing twice with TDB-glucose at room temperature. Suspensions were centrifuged
375 at 1000 g for 5 min and pipetted into 6-well microscope slides and dried at RT. Cells were
376 fixed with 25µl 2% paraformaldehyde diluted in PBS and incubated at room temperature for
377 5 min. Cells were washed in PBS to remove paraformaldehyde prior to washing twice more
378 with PBS and permeabilized with 0.05% NP40 for 10 min. Cells were washed twice in PBS

379 and dried at RT. Mounting media with DAPI was added to each well with a coverslip. Slides
380 were kept at 4 °C before viewing using a Zeiss LSM 880 with Airyscan on an Axio
381 Observer.Z1 invert confocal microscope.

382 For cell cycle analysis, bloodstream form *T. brucei* cell lines were incubated or not for 6 hr
383 with AB compounds at a final concentration of 2X and 5X the individual EC₅₀ value for each
384 compound (averaged from viability assays). Control cultures were treated with 0.5µl DMSO
385 but no AB compound. Cultures were pelleted and cells were collected and washed once in
386 *Trypanosoma* dilution buffer (TDB) supplemented with 5 mM of EDTA and resuspended in
387 70% methanol. Cells were centrifuged at 1400 g for 10 min to remove methanol and washed
388 once in TDB 1x with 5mM EDTA. Cells were resuspended in 1ml TDB 1x with 5mM
389 EDTA, 10µg ml⁻¹ of propidium iodide and 10µl of RNase A. Cell suspensions in 1.5 ml tubes
390 were wrapped in foil to avoid bleaching by light. Cells were incubated for 30 min at 37°C in
391 the dark until FACS analysis. Cells were analysed for FACS using a Beckman Coulter CyAn
392 ADP flow cytometer (excitation; 535, emission; 617).

393

394 In the cell cycle analysis, CLK1 OE was induced during 18 hr with tetracycline (1 µg ml⁻¹)
395 and later treated with 4X the individual EC₅₀ value for each compound for 4 hr (maintaining
396 tetracycline induction), and finally collected for flow cytometry as above.

397

398 Parasite cell sorting was conducted as described previously¹⁹. Briefly, cell lines were
399 harvested during exponential growth by centrifugation for 10 min at room temperature. The
400 parasite pellet was then resuspended at a concentration of 1 × 10⁶ cells ml⁻¹ in HMI-9
401 medium supplemented with 2% FCS and 10 µg ml⁻¹ penicillin/streptomycin. Vybrant
402 DyeCycle Violet (Molecular Probes, Invitrogen) was added to a final concentration of 1 µg
403 ml⁻¹ and the cell suspension incubated for 30 min at 37 °C, the tube being protected from light
404 by wrapping in aluminium foil. The samples were then centrifuged and resuspended back in
405 the staining media prior to sorting on a MoFlo XDP Sorter (Beckman Coulter Life Sciences).
406 During and after the sorting, the samples were cooled to below 20 °C to limit cell metabolic
407 activity. The dye was excited using a 407 nm Violet laser and emission detected via a 450/40
408 bandpass filter. Live parasites were gated based on FSC/SSC profiles, and the gates were set
409 up to collect only the 2C fraction (G0/G1 cells) and 4C fraction (G2, mitotic and post-mitotic
410 cells), to ensure efficient discrimination and selection of these cell-cycle stages.

411

412 **Protein analysis**

413 Biochemical assays for human EGFR (Epidermal growth factor receptor) and BTK (Bruton's
414 tyrosine kinase) were carried out using a homogenous time-resolved fluorescence (HTRF)
415 assay as described previously⁸.

416 For enzyme purification, full-length TbCLK1 (Q382U0) CDS was cloned in pET28a PreSc-
417 His and pET24-MBP-TEV vector respectively. Human CLK1 (hCLK1; P49759) was
418 obtained from Promega. Recombinant expression was carried out by lactose autoinduction in
419 Terrific Broth containing 0.4% glycerol, 0.05% glucose, 0.05% lactose, 0.05% arabinose and
420 buffered by 100 mM sodium phosphate (pH 7.0). In brief, 0.7 L of this media (in a 2.8 L
421 Fernbach flask) was inoculated at 0.1 OD600 with an overnight Luria Broth culture and
422 shaken at 37 °C and 250 rpm for 2.5 hr. Then, temperature was lowered to 18 °C and the
423 culture was allowed to grow and induced overnight and harvested 20-24 hr later. Cells were
424 pelleted and stored at -80 °C prior to purification. Cell lysis was done by sonication in an ice
425 bath (20 sec ON/OFF, 3 min active sonication at 70-110 watts power) in 40 mL equilibration
426 buffer (25 mM HEPES pH 7.5 300 mM NaCl 5% glycerol 0.5 mM TCEP) and the clarified
427 lysate is purified by IMAC on a 5 mL HisTrap column (GE Healthcare). The IMAC elution
428 was further purified by sizing on a 300 mL Superdex 200 prep grade column (GE Healthcare)
429 packed in a 2.6 cm diameter housing. Included volume fractions were pooled and analysed by
430 SDS-PAGE or LC-MS.

431 Preliminary characterization of the TbCLK1 enzyme was carried out and the Km for ATP
432 and MBP (Myelin basic protein, dephosphorylated, Sigma-Aldrich Catalogue no: 13-110,
433 LOT: 3107375) substrate was found to be $9.3 \pm 3.6 \mu\text{M}$ and $0.065 \pm 0.02 \text{ mg ml}^{-1}$,
434 respectively. TbCLK1 and hCLK1 enzyme activity assays were performed in white 384 well,
435 solid bottom, Small Volume™ plates (GREINER). The assay buffer contained 40 mM Tris
436 (pH 7.5), 20 mM MgCl₂, 0.1mg/ml BSA and 2 mM DTT. Each enzyme (TbCLK1 = 3 nM;
437 hCLK1 = 50 nM) was first incubated with different compound serial dilutions or DMSO
438 control during 10 min and then ATP (10 μM) and MBP substrate (0.1 mg ml⁻¹) mixture was
439 added to initiate the reaction. After 30 min reaction at room temperature, the ADP-Glo
440 reagent and detection solution were added following the technical manual of ADP-Glo™
441 kinase assay kit (Promega). The luminescence was measured on CLARIOstar BMG
442 LABTECH microplate reader. In all the assays, staurosporine was used as positive control of
443 inhibition. Apparent IC₅₀ values were plotted using GraphPad Prism software. The co-crystal

444 structure of TbCLK1 with AB1 showed specific covalent interaction with cysteine 215. It
445 may be possible that all AB series compounds with Michael acceptors have covalent
446 inhibition of TbCLK1. Since biochemical SAR analysis for all AB series compounds was
447 carried out beyond 10 min incubation with rCLK1, IC₅₀s are represented as apparent IC₅₀s.
448 The AB1 compound showed time dependent inhibition of rCLK1 wherein IC₅₀ plateaued
449 around 20 min.

450 For Western blotting parasites were washed with trypanosome dilution buffer (TDB)
451 supplemented with 20 mM glucose. After centrifugation, the samples were resuspended in the
452 RIPA buffer (New England Biolabs) supplemented with protease and phosphatase inhibitors
453 obtained from Promega and Roche Life Science respectively. All samples were quantified by
454 *Bradford protein* assay (Bio-Rad), 25 µg of protein was loaded, resolved in a 4-20%
455 NuPAGE Bis-Tris gel (Invitrogen) in NuPAGE MOPS running buffer and transferred onto
456 Hybond-C nitrocellulose membranes (GE Healthcare) at 350 mA for 2 hr or, for high
457 molecular weight proteins, overnight at 4 °C.

458 After transfer, membranes were washed once in 1x TBST (tris-*buffered* saline (TBS), 0.01%
459 Tween-20 (Sigma Aldrich)) for 10 min then incubated for 1 hr in blocking solution (1x
460 TBST, 5% BSA) or, if required, overnight at 4 °C. Next, the membrane was rinsed for 10 min
461 in 1X TBST and placed in blocking buffer containing the required primary antisera for 1 hr at
462 room temperature or overnight at 4 °C. The membrane was then washed 3 times with TBST
463 and placed in blocking solution containing the appropriate fluorescent secondary antisera for
464 1 hr. A list of antibodies is provided in Supplementary Methods.

465

466 **Determination of solubility, plasma protein binding, brain tissue binding and** 467 **microsomal clearance.**

468 Solubility of AB0 and AB1 compounds were determined in a high-throughput
469 thermodynamic solubility assay as described previously³⁴. Plasma protein binding was
470 determined for AB1 using mouse blood³⁴, whilst brain tissue binding was determined using
471 rat brain tissues. Intrinsic metabolic clearance of AB0 and AB1 were determined in mouse,
472 rat and human liver microsomes using the compound depletion approach and LC-MS/MS
473 quantification³⁵.

474 **Crystallization, data collection, and structure determination.**

475 The TbCLK1/AB1 complex was formed by incubating TbCLK1 kinase domain (V117-
476 M465) with 1mM AB1 at room temperature for 2 hours. The excess AB1 was removed by
477 dialysis overnight in buffer containing 25mM HEPES pH 7.5, 250mM NaCl, 0.5mM TCEP.
478 The TbCLK1 kinase domain/AB1 complex was concentrated to 15 mg/ml for crystallization
479 trials. Crystallization experiments were carried out at 4°C using the sitting-drop vapor
480 diffusion setup. Crystals of the TbCLK1 kinase domain/AB1 complex grew out of a well
481 containing 0.1M HEPES pH 7.5, 1.6M Ammonium Sulfate, 2% w/v Peg 1000. Crystals were
482 cryo-protected in reservoir solution supplemented with 20% glycerol and flash-cooled in
483 liquid nitrogen for data collection. Datasets were collected under cryogenic conditions
484 (100K) at the Advanced Light Source (ALS) beamline 5.0.2. All data were processed using
485 Xia2³⁶, employing XDS³⁷ for data integration and AIMLESS³⁸ for scaling. Molecular
486 replacement were carried out using PHASER³⁹ with coordinates from human CLK1 crystal
487 structure (PDB ID 6FT8)⁴⁰. Structure refinement was carried out in PHENIX⁴¹ alternated
488 with manual fitting in Coot⁴². Data collection and structure refinement statistics are included
489 in Extended data Table 1.

490 **Differential Scanning Fluorimetry (DSF) for CLK1**

491 Scanning fluorimetry (DSF) was performed on an Applied Biosystems Viia 7 RT PCR
492 instrument, and data was analyzed using Protein Thermal Shift Software version 1.3 (Applied
493 Biosystems/Thermo Fisher). Recombinant *Trypanosoma brucei* CLK1 wild-type or C215A
494 protein was diluted to 5 µM in 25 mM 4-(2-Hydroxyethyl)piperazine-1-ethanesulfonic acid,
495 N-(2-Hydroxyethyl)piperazine-N'-(2-ethanesulfonic acid) (HEPES) pH 7.5 300 mM NaCl
496 5% glycerol and 1 mM Tris(2-carboxyethyl)phosphine hydrochloride (TCEP). Compounds in
497 DMSO or DMSO control was added to a final concentration of 2 mM DMSO and 50 µM
498 compound. SYPRO Orange (Invitrogen/Thermo Fisher) was pre-diluted to 100x in the
499 protein buffer and added to a final concentration of 10x. 70 µl of each condition was
500 prepared. After 30 min of incubation, 3x 20 µl was aliquoted bubble-free into a 384 well PCR
501 plate and covered with RT PCR compatible film, then centrifuged 10 min at 2000 rpm at
502 room temperature, and read in the RT PCR instrument with the appropriate filters. The
503 thermal shift program consisted of 3 minutes at 25 °C followed by a 25-95 °C ramp at 0.03
504 °C/second and 5 seconds at 95 °C.

505 **General Statistics.**

506 All statistical analysis was performed using GraphPad Prism 8
507 (<http://www.graphpad.com/scientific-software/prism/>). The appropriate tests were conducted
508 and are as detailed in the corresponding figure legends.

509 **Acknowledgments**

510 This work was supported by the Wellcome Trust (069712, 103024 and 108517). JCM is a
511 Wellcome Trust Investigator (200807). MPB and JCM are part of the Wellcome Centre of
512 Integrative Parasitology (104111/Z/14/Z). We thank our colleagues in The Bioscience
513 Technology Facility of University of York who provided insight and expertise that greatly
514 assisted our microscopy and flow cytometry research. We thank Gerald Lelais, Vanessa
515 Manoharan, Rima Palkar, Vivian Lim, Christian Noble and Wan Kah Fei for their technical
516 support.

517 **Bibliography**

- 518 1. World Health Organization. *Integrating neglected tropical diseases into global health*
519 *and development: fourth World Health Organization report on neglected tropical*
520 *diseases*. (apps.who.int, 2017).
- 521 2. Mesu, V. K. B. K. *et al.* Oral fexinidazole for late-stage African *Trypanosoma brucei*
522 *gambiense* trypanosomiasis: a pivotal multicentre, randomised, non-inferiority trial.
523 *Lancet* **391**, 144–154 (2018).
- 524 3. Dickie, E. A. *et al.* New drugs for human african trypanosomiasis: A twenty first century
525 success story. *TropicalMed* **5**, (2020).
- 526 4. Khare, S. *et al.* Proteasome inhibition for treatment of leishmaniasis, Chagas disease and
527 sleeping sickness. *Nature* **537**, 229–233 (2016).
- 528 5. Wyllie, S. *et al.* Cyclin-dependent kinase 12 is a drug target for visceral leishmaniasis.
529 *Nature* **560**, 192–197 (2018).
- 530 6. Rao, S. P. S. *et al.* Drug discovery for kinetoplastid diseases: future directions. *ACS*
531 *Infect. Dis.* **5**, 152–157 (2019).
- 532 7. Myburgh, E. *et al.* In vivo imaging of trypanosome-brain interactions and development
533 of a rapid screening test for drugs against CNS stage trypanosomiasis. *PLoS Negl. Trop.*
534 *Dis.* **7**, e2384 (2013).
- 535 8. Lelais, G. *et al.* Discovery of (R,E)-N-(7-Chloro-1-(1-[4-(dimethylamino)but-2-
536 enoyl]azepan-3-yl)-1H-benzo[d]imidazol-2-yl)-2-methylisonicotinamide (EGF816), a
537 Novel, Potent, and WT Sparing Covalent Inhibitor of Oncogenic (L858R, ex19del) and
538 Resistant (T790M) EGFR Mutants for the Treatment of EGFR Mutant Non-Small-Cell
539 Lung Cancers. *J. Med. Chem.* **59**, 6671–6689 (2016).

- 540 9. Parsons, M., Worthey, E. A., Ward, P. N. & Mottram, J. C. Comparative analysis of the
541 kinomes of three pathogenic trypanosomatids: *Leishmania major*, *Trypanosoma brucei*
542 and *Trypanosoma cruzi*. *BMC Genomics* **6**, 127 (2005).
- 543 10. Begolo, D., Erben, E. & Clayton, C. Drug target identification using a trypanosome
544 overexpression library. *Antimicrob. Agents Chemother.* **58**, 6260–6264 (2014).
- 545 11. McNamara, C. W. *et al.* Targeting Plasmodium PI(4)K to eliminate malaria. *Nature* **504**,
546 248–253 (2013).
- 547 12. Moeslein, F. M., Myers, M. P. & Landreth, G. E. The CLK family kinases, CLK1 and
548 CLK2, phosphorylate and activate the tyrosine phosphatase, PTP-1B. *J. Biol. Chem.* **274**,
549 26697–26704 (1999).
- 550 13. Jones, N. G. *et al.* Regulators of *Trypanosoma brucei* cell cycle progression and
551 differentiation identified using a kinome-wide RNAi screen. *PLoS Pathog.* **10**, e1003886
552 (2014).
- 553 14. Akiyoshi, B. & Gull, K. Discovery of unconventional kinetochores in kinetoplastids.
554 *Cell* **156**, 1247–1258 (2014).
- 555 15. Nishino, M., Choy, J. W., Gushwa, N. N. & Oses-Prieto, J. A. Hypothemycin, a fungal
556 natural product, identifies therapeutic targets in *Trypanosoma brucei*. *Elife* (2013).
- 557 16. Liu, Q. *et al.* Developing irreversible inhibitors of the protein kinase cystinome. *Chem.*
558 *Biol.* **20**, 146–159 (2013).
- 559 17. Westhorpe, F. G. & Straight, A. F. Chromosome segregation: reconstituting the
560 kinetochore. *Curr. Biol.* **26**, R1242–R1245 (2016).
- 561 18. D’Archivio, S. & Wickstead, B. Trypanosome outer kinetochore proteins suggest
562 conservation of chromosome segregation machinery across eukaryotes. *J. Cell Biol.* **216**,
563 379–391 (2017).
- 564 19. Kabani, S., Waterfall, M. & Matthews, K. R. Cell-cycle synchronisation of bloodstream
565 forms of *Trypanosoma brucei* using Vybrant DyeCycle Violet-based sorting. *Mol.*
566 *Biochem. Parasitol.* **169**, 59–62 (2010).
- 567 20. Torrie, L. S. *et al.* Identification of inhibitors of an unconventional *Trypanosoma brucei*
568 kinetochore kinase. *PLoS One* **14**, e0217828 (2019).
- 569 21. Ishii, M. & Akiyoshi, B. Characterization of unconventional kinetochore kinases
570 KKT10/19 in *Trypanosoma brucei*. *J. Cell Sci.* (2020). doi:10.1242/jcs.240978
- 571 22. Mackey, Z. B., Koupparis, K., Nishino, M. & McKerrow, J. H. High-throughput analysis
572 of an RNAi library identifies novel kinase targets in *Trypanosoma brucei*. *Chem Biol*
573 *Drug Des* **78**, 454–463 (2011).
- 574 23. Roskoski, R. Properties of FDA-approved small molecule protein kinase inhibitors.
575 *Pharmacol. Res.* **144**, 19–50 (2019).
- 576 24. Wyllie, S. *et al.* Preclinical candidate for the treatment of visceral leishmaniasis that acts
577 through proteasome inhibition. *Proc. Natl. Acad. Sci. USA* **116**, 9318–9323 (2019).

- 578 25. Alam, M. M. *et al.* Validation of the protein kinase PfCLK3 as a multistage cross-species
579 malarial drug target. *Science* **365**, (2019).
- 580 26. van Hooff, J. J., Tromer, E., van Wijk, L. M., Snel, B. & Kops, G. J. Evolutionary
581 dynamics of the kinetochore network in eukaryotes as revealed by comparative
582 genomics. *EMBO Rep.* **18**, 1559–1571 (2017).
- 583 27. Duncan, S. M. *et al.* Conditional gene deletion with DiCre demonstrates an essential role
584 for CRK3 in *Leishmania mexicana* cell cycle regulation. *Mol. Microbiol.* **100**, 931–944
585 (2016).
- 586 28. Buckner, F. S., Verlinde, C. L., La Flamme, A. C. & Van Voorhis, W. C. Efficient
587 technique for screening drugs for activity against *Trypanosoma cruzi* using parasites
588 expressing beta-galactosidase. *Antimicrob. Agents Chemother.* **40**, 2592–2597 (1996).
- 589 29. Alsford, S., Kawahara, T., Glover, L. & Horn, D. Tagging a *T. brucei* RRNA locus
590 improves stable transfection efficiency and circumvents inducible expression position
591 effects. *Mol. Biochem. Parasitol.* **144**, 142–148 (2005).
- 592 30. Dean, S., Sunter, J. D. & Wheeler, R. J. TrypTag.org: A Trypanosome Genome-wide
593 Protein Localisation Resource. *Trends Parasitol.* **33**, 80–82 (2017).
- 594 31. Kaiser, M. *et al.* Antitrypanosomal activity of fexinidazole, a new oral nitroimidazole
595 drug candidate for treatment of sleeping sickness. *Antimicrob. Agents Chemother.* **55**,
596 5602–5608 (2011).
- 597 32. Alsford, S. & Horn, D. Single-locus targeting constructs for reliable regulated RNAi and
598 transgene expression in *Trypanosoma brucei*. *Mol. Biochem. Parasitol.* **161**, 76–79
599 (2008).
- 600 33. Thuita, J. K. *et al.* Efficacy of the diamidine DB75 and its prodrug DB289, against
601 murine models of human African trypanosomiasis. *Acta Trop.* **108**, 6–10 (2008).
- 602 34. Waters, N. J., Jones, R., Williams, G. & Sohal, B. Validation of a rapid equilibrium
603 dialysis approach for the measurement of plasma protein binding. *J. Pharm. Sci.* **97**,
604 4586–4595 (2008).
- 605 35. Kalvass, J. C., Tess, D. A., Giragossian, C., Linhares, M. C. & Maurer, T. S. Influence of
606 microsomal concentration on apparent intrinsic clearance: implications for scaling in
607 vitro data. *Drug Metab. Dispos.* **29**, 1332–1336 (2001).
- 608 36. Winter, G. Xia2 : an expert system for macromolecular crystallography data reduction. *J*
609 *Appl Crystallogr* **43**, 186–190 (2010).
- 610 37. Kabsch, W. XDS. *Acta Crystallogr. Sect. D, Biol. Crystallogr.* **66**, 125–132 (2010).
- 611 38. Evans, P. R. & Murshudov, G. N. How good are my data and what is the resolution?
612 *Acta Crystallogr. Sect. D, Biol. Crystallogr.* **69**, 1204–1214 (2013).
- 613 39. McCoy, A. J. *et al.* Phaser crystallographic software. *J Appl Crystallogr* **40**, 658–674
614 (2007).

- 615 40. Walter, A. *et al.* Molecular structures of cdc2-like kinases in complex with a new
616 inhibitor chemotype. *PLoS One* **13**, e0196761 (2018).
- 617 41. Adams, P. D. *et al.* PHENIX: a comprehensive Python-based system for macromolecular
618 structure solution. *Acta Crystallogr. Sect. D, Biol. Crystallogr.* **66**, 213–221 (2010).
- 619 42. Emsley, P., Lohkamp, B., Scott, W. G. & Cowtan, K. Features and development of Coot.
620 *Acta Crystallogr. Sect. D, Biol. Crystallogr.* **66**, 486–501 (2010).

621

622 **Figure legends**

623 **Fig. 1 Pan kinetoplastid activity of amidobenzimidazole (AB) series.**

- 624 (a) Structure, anti-kinetoplastid parasite activity, cytotoxicity, tyrosine kinase inhibition
625 and *in vitro* pharmacokinetics of AB0 and AB1. EC₅₀ and CC₅₀ represent half-
626 maximum growth inhibition concentration. hEGFR: human epidermal growth factor
627 receptor enzyme. BTK: Bruton's tyrosine kinase. IC₅₀ represents half-maximum
628 enzyme inhibition concentration. All the cellular and biochemical data presented were
629 generated with minimum of n=2 or more independent biological replicates (each
630 biological replicate had n=2 technical replicates). All physicochemical and *in vitro*
631 pharmacokinetics experiments were carried out with at least n = 4 technical replicates
632 (except for rat microsomal clearance for AB0, which had n =2 technical replicates).
- 633 (b) Structure activity relationship of amidobenzimidazoles. Each dot represents one
634 compound. Compounds with the Michael acceptor (orange circles) were more potent
635 against *T. b. brucei* (Tbb pEC₅₀) and had better lipophilic efficiency (clogP, calculated
636 octanol-water partition coefficient) compared to non-Michael acceptor compounds
637 (blue circles). AB0 (dark blue) and AB1 (dark orange). The Tbb pEC₅₀ data are the
638 negative logarithm of 50% growth inhibition of bloodstream form of *T. b. brucei*
639 (minimum n = 2 biological replicates). The compounds on the left side of the two
640 slanted dotted lines represent lipophilic ligand efficiency (LipE) of 3 and 4. The
641 compounds above two horizontal dotted lines have EC₅₀ of 1000 and 100 nM against
642 bloodstream form *T. b. brucei*.
- 643 (c) *In vivo* activity of AB1 in a haemolympathic mouse model for human African
644 trypanosomiasis (untreated control group, mice = 4; all the other experimental groups,
645 mice = 6). Each group of mice were infected with *T. b. brucei* and 3 days post
646 infection, mice were treated with varying concentration of AB1 for 4 days once daily
647 and monitored for relapse in parasitemia over a period of 31 days. Cure plot (Kaplan-
648 Meier plot) showing percentage of animals cured over time are shown. Note the dose
649 dependent activity of AB1, achieving complete cure at 50 mg kg⁻¹ once daily dose (in
650 violet).

651

652 **Fig. 2 Identification of CLK1 as the molecular target for the AB series.**

- 653 (a) Inducible overexpression (OE) of essential protein kinases (PKs) and target
654 deconvolution approach for the AB series. Schematic representation of the
655 experimental workflow: 6-myc OE plasmids, each containing a specific protein kinase
656 tagged with six myc epitopes, were individually transfected into 2T1 bloodstream

657 form *T. b. brucei* (VSG221 expressing, Tagged, clone 1). Viability of induced
658 individual *T. b. brucei* OE lines after treatment was assessed by measuring the
659 conversion of resazurin (Alamar blue) to resorufin.

660 (b) AB1 half-maximal effective concentration (EC₅₀) was analysed from twenty-nine
661 essential individual protein kinase over-expression cell lines (dark grey circles). The
662 graph represents EC₅₀ fold change over the parental cell line (*T. b. brucei* 2T1 cell
663 line, DMSO) (light grey shade box), where overexpression of CLK1 confers
664 resistance to AB1. The grey bar represents the EC₅₀ average of all cell lines over
665 control. Box error bars represent the library mean with 95% of confidence interval of
666 two biological replicates of the library and CLK1 (n = 4 biological replicates). P-
667 value was calculated using two-tailed Student's t-tests comparing CLK1 OE with
668 parental cell line where *** p-value = 5×10^{-5} .

669 (c) CLK1 over-expression confers resistance to AB1-induced cell cycle arrest. CLK1
670 over-expression was induced or not with tetracycline for 18 h, and cells then
671 incubated for 6 h with 5x AB1 EC₅₀ (dark grey bars); the 2T1 cell line was a parental
672 control. Cell cycle distribution was determined by flow cytometry. Left: dotted line
673 represents (basal) G2/M untreated average and *** represents a p-value = 1.2×10^{-4}
674 (2T1 untreated vs AB1), p-value = 5.8×10^{-4} (CLK1 OE uninduced vs AB1), and not
675 significant (ns) p-value = 0.02 (CLK1 OE induced vs AB1). P-value was calculated
676 using two-tailed Student's t-test. Error bars represent mean \pm SEM of three biological
677 replicates, Right: representative cell cycle profile histogram of cells stained with
678 propidium iodide showing G2/M cell cycle accumulation (arrow).

679 (d) Violin plot of average length (μm) of the nuclei from parasites treated (blue) or not
680 (grey) with AB1 (n=160 2K1N parasites, *** p-value = 3.9×10^{-26}). Dashed line
681 represents the mean value, and dotted lines indicate both quartiles (25th & 75th). P-
682 value was calculated using unpaired two-tailed Student's t-test. Right: Example of a
683 cell stained with DAPI (cyan) from each condition, where N= nucleus, K=
684 Kinetoplast.

685 (e) Cell cycle analysis of synchronized *T. b. brucei* after treatment with AB1. Top:
686 Kinetoplast/nucleus configuration of 2C and 4C synchronized parasites, treated or not
687 with 5x EC₅₀ AB1 was quantified by DAPI staining at the indicated points (n=200
688 cells). K = kDNA, N = nucleus, D = duplicating kDNA. Bottom: Schematic
689 representation of *T. brucei* kinetoplast/nucleus configuration through the cell cycle.

690
691 **Fig. 3 Mechanism of CLK1 inhibition by AB1**

692 (a) Positive correlation between inhibition of recombinant *T. brucei* CLK1 enzyme
693 (apparent pIC₅₀) and growth inhibition (pEC₅₀) of *T. b. brucei* bloodstream form
694 parasites with AB series compounds (n=260; Pearson correlation coefficient (r) =
695 0.68. Presence (orange) or absence (blue) of Michael acceptor pharmacophore is
696 shown, highlighting AB1 (dark orange) and AB0 (dark blue). Black dash line
697 represents equimolar potency and grey dash line represents 10-fold higher potency for
698 CLK1 pIC₅₀ compared to Tbb pEC₅₀.

699 (b) Lack of correlation between inhibition of recombinant human CLK1 (hCLK1) and
700 recombinant *T. brucei* CLK1 enzyme (apparent pIC₅₀) with AB compound series
701 (n=228; Pearson correlation coefficient (r) = 0.03). Majority of compounds showed >
702 10-fold selectivity against TbCLK1 compared to hCLK1. Presence (orange) or

703 absence (blue) of Michael acceptor pharmacophore is shown, highlighting AB1 (dark
704 orange) and AB0 (dark blue). Grey dash line represents equimolar potency and black
705 dash line represents 10-fold higher potency for CLK1 pIC₅₀ compared to hCLK1
706 pIC₅₀.

707 (c) Crystal structure of the *T. brucei* CLK1 kinase domain (V117-M465) in a covalent
708 thioether bond with AB1 at C215 (PDB: 6Q2A). The CLK1 kinase domain is shown
709 in grey, with a blue α C helix, and the side chains of the DFG motif (DLG in CLK1)
710 shown as sticks. Inhibitor AB1 is shown as ball and sticks with carbon coloured
711 purple, oxygen coloured red and nitrogen coloured blue. A semi-transparent
712 representation of AB1 van der Waals surfaces are shown in magenta. Inset depicts the
713 detailed view of the interactions of AB1. Hydrogen bonds and salt bridge are shown
714 as dotted blue line. MAP-like insertion is showed in orange.

715 (d) Omit 2Fo-Fc map of AB1/C215 at 2.6Å resolution contoured at 2 σ . Hydrogen bonds
716 and salt bridge between the AB1 molecule and *T. brucei* bCLK1 are drawn as blue
717 lines. Covalent bond indicated by yellow arrow.

718

719 **Fig. 4 CLK1 is the primary target for AB1 in bloodstream form trypanosomes**

720 (a) AB1 binding to CLK1, as probed via differential scanning fluorimetry (DSF).
721 Thermal unfolding of CLK1 is monitored by SYPRO Orange. CLK1 WT (left) and
722 CLK1 C215A (right) recombinant protein in the presence of AB0 (green), AB1 (red)
723 or DMSO (blue) as a reference. Data from one representative experiment, out of three
724 independent experiment with similar results, are shown. Note the shift in T_m (melting
725 temperature of protein) for CLK1 in presence of AB1 compound.

726 (b) Expression of *T. brucei* CLK1 C215A mutant is resistant to AB1. Dose-response
727 curves of apparent AB1 and staurosporine IC₅₀ of recombinant WT *T. brucei* CLK1
728 and C215A mutant. Response to 3-fold serial dilutions of each compound were
729 assessed as described in methods. Each data point represents the mean of two
730 technical replicates.

731 (c) Overexpression of CLK1 C215S mutant confers > 60-fold EC₅₀ shift to AB1. CLK1
732 C215S mutation (green) was overexpressed in the parental *T. b. brucei* 2T1 cell line
733 and AB1 half-maximal effective concentration (EC₅₀) was determined after 72 h and
734 compared with *T. b. brucei* 2T1 WT parental cell line (blue). Data represent mean \pm
735 SEM of three independent biological experiments. Inset: Tetracycline inducible over-
736 expression of CLK1-myc was assessed for three clones by western blot, using an anti-
737 myc antibody. EF1 α was used as the loading control.

738 (d) Overexpression of CLK1 C215S mutant impairs the parasite growth effect of AB1
739 treatment. Parasites overexpressing CLK1 C215S (green) and parental *T. b. brucei*
740 2T1 cell line (blue) were treated with 5x (line) or 10x AB1 EC₅₀ (dashed line) during
741 48 h. Mean \pm SEM (n=3) is shown. Data represent the mean of the percentage of cell
742 growth relative to time=0 h (1.5×10^4 parasites ml⁻¹). P values were calculated using a
743 two-tailed Student's t-test comparing with parental control where *** represent the P-
744 values of 24 h (p-value = 5.4×10^{-4}), 48 h (p-value = 3.4×10^{-4}), and 72 h (p-value =
745 3.3×10^{-4}) after treatment with 5x AB1 EC₅₀, and 24 h (p-value = 9.9×10^{-7}), 48 h (p-
746 value = 1.7×10^{-3}), and 72 h (p-value = 1.6×10^{-3}) for 10x AB1 EC₅₀ treatment.

747 (e) Percentage of survival of parasites exposed to 5-150x AB1 EC₅₀ fold range. Parental
748 *T. b. brucei* 2T1 control (blue) and CLK1 C215S mutant (green) (2×10^3 parasites ml⁻¹)
749 were exposed for 72 h to 5, 15, 50, and 150-fold AB1 EC₅₀. Survival was calculated
750 by using CellTiter-Glo® luminescent cell viability assay. Data represent the mean ±
751 SEM of percentage of survival. (C215S mutant n=3, Parental 2T1 n=4).

752 **Fig. 5 CLK1 inhibition impairs inner kinetochore dynamics.**

753 (a) Localization of kinetochore protein KKT2 after CLK1 inhibition by AB1. Parasites
754 were incubated or not for 24 h with 2x EC₅₀ (upper panel) or 6 h with 5 x EC₅₀ AB1
755 (lower panel). Representative fluorescence micrographs, showing bloodstream form
756 parasites endogenously expressing N-terminal mNeonGreen (mNG) tagged KKT2.
757 Cells in metaphase and anaphase are shown. Cells were counterstained with DAPI to
758 visualize DNA (cyan). The right panel shows the Nomarsky (DIC) corresponding
759 images. Upper right panel shows cell cycle progression after treatment with 2x EC₅₀
760 AB1 for 72 h. Data are representative from one of three independent biological
761 replicates with similar results.

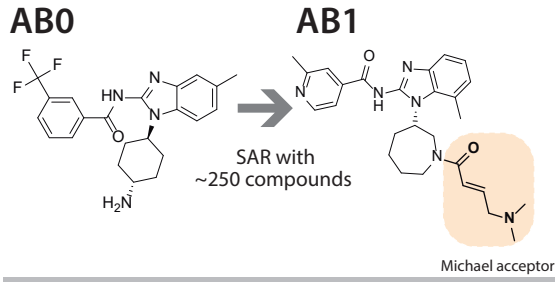
762 (b) Localization of KKT2 after CLK1 depletion by RNAi. Representative fluorescence
763 micrographs, showing 24 h induction of CLK1 RNAi in bloodstream form parasites
764 endogenously expressing N-terminal mNeonGreen (mNG) labelled KKT2, compared
765 with not induced control cells in metaphase and anaphase are shown. Cells were
766 counterstained with DAPI to visualize DNA (cyan). The right panel shows the
767 Nomarsky (DIC) corresponding images. Data are representative from one of three
768 independent biological replicates with similar results.

769

770

Figure 1

a



Cellular activity [μM]

<i>T. brucei brucei</i> EC ₅₀	0.29 ± 0.014	0.072 ± 0.006
<i>T. b. gambiense</i> EC ₅₀	0.37 ± 0.072	0.057 ± 0.013
<i>T. b. rhodesiense</i> EC ₅₀	-	0.033 ± 0.009
<i>T. cruzi</i> EC ₅₀	1.27 ± 0.052	0.044 ± 0.017
<i>L. donovani</i> EC ₅₀	-	0.600 ± 0.078
<i>L. mexicana</i> EC ₅₀	-	1.564 ± 0.045
NIH 3T3 fibroblast CC ₅₀	4.38 ± 0.79	9.660 ± 2.240
HepG2 CC ₅₀	2.35 ± 0.24	9.060 ± 0.830

Tyrosine Kinase activity [μM]

hEGFR IC ₅₀	0.3*	0.002 ± 0.0005
BTK IC ₅₀	-	0.002 ± 0.0025

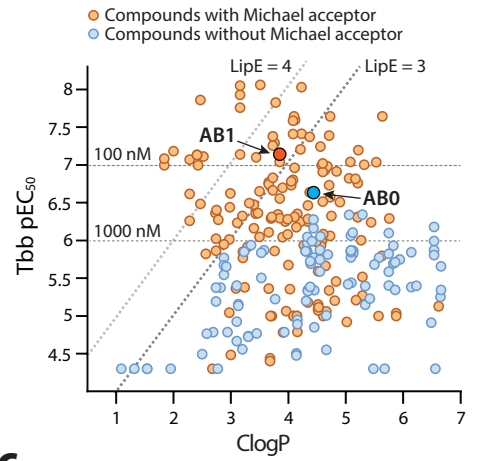
Physicochemical and *in vitro* Pharmacokinetics

Solubility [μM]	32,85 ± 0.01	900 ± 8.165
Plasma protein binding [%]	-	94.1 ± 0.100
Brain tissue binding [μM]	-	>99
Microsomal clearance (mice/rat/human) [$\mu\text{l}/\text{min}/\text{mg}$]	42.4 ± 1.19/184*/27 ± 20.1	65.5 ± 3.2/22.2 ± 3.9/42.4 ± 15.6

▲ Bloodstream form, ▲▲ Intracellular amastigote, ▲▲▲ Axenic amastigote.

*Data obtained from two technical replicates

b



c

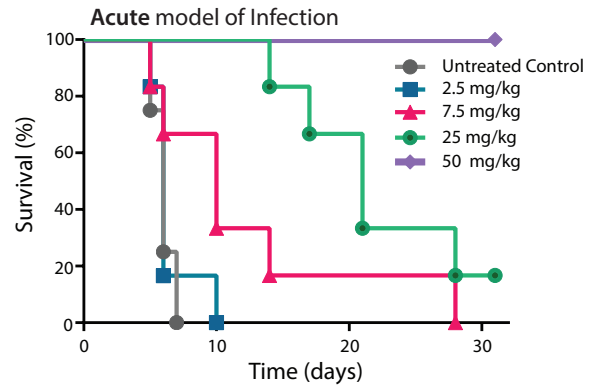


Figure 3

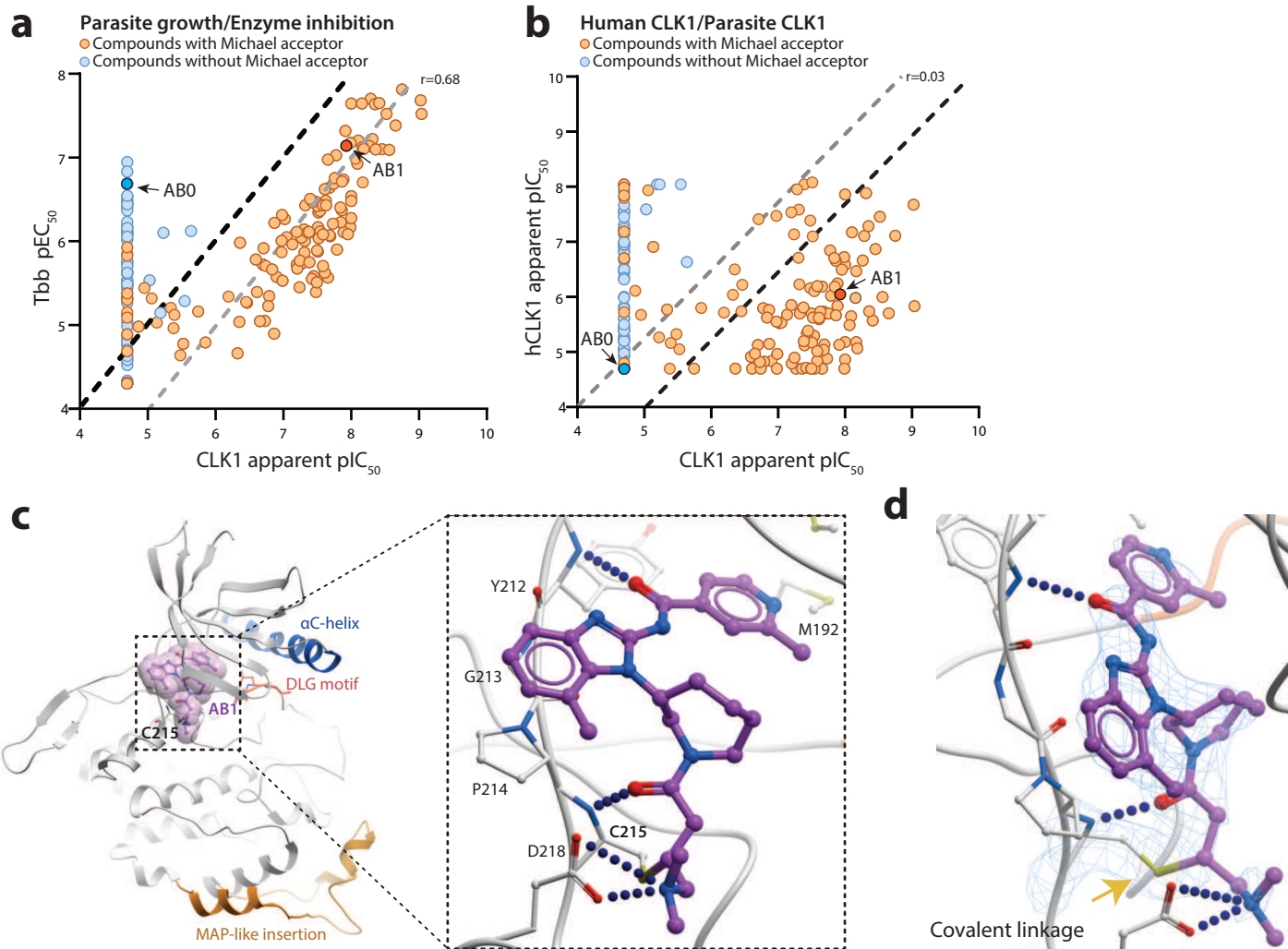


Figure 4

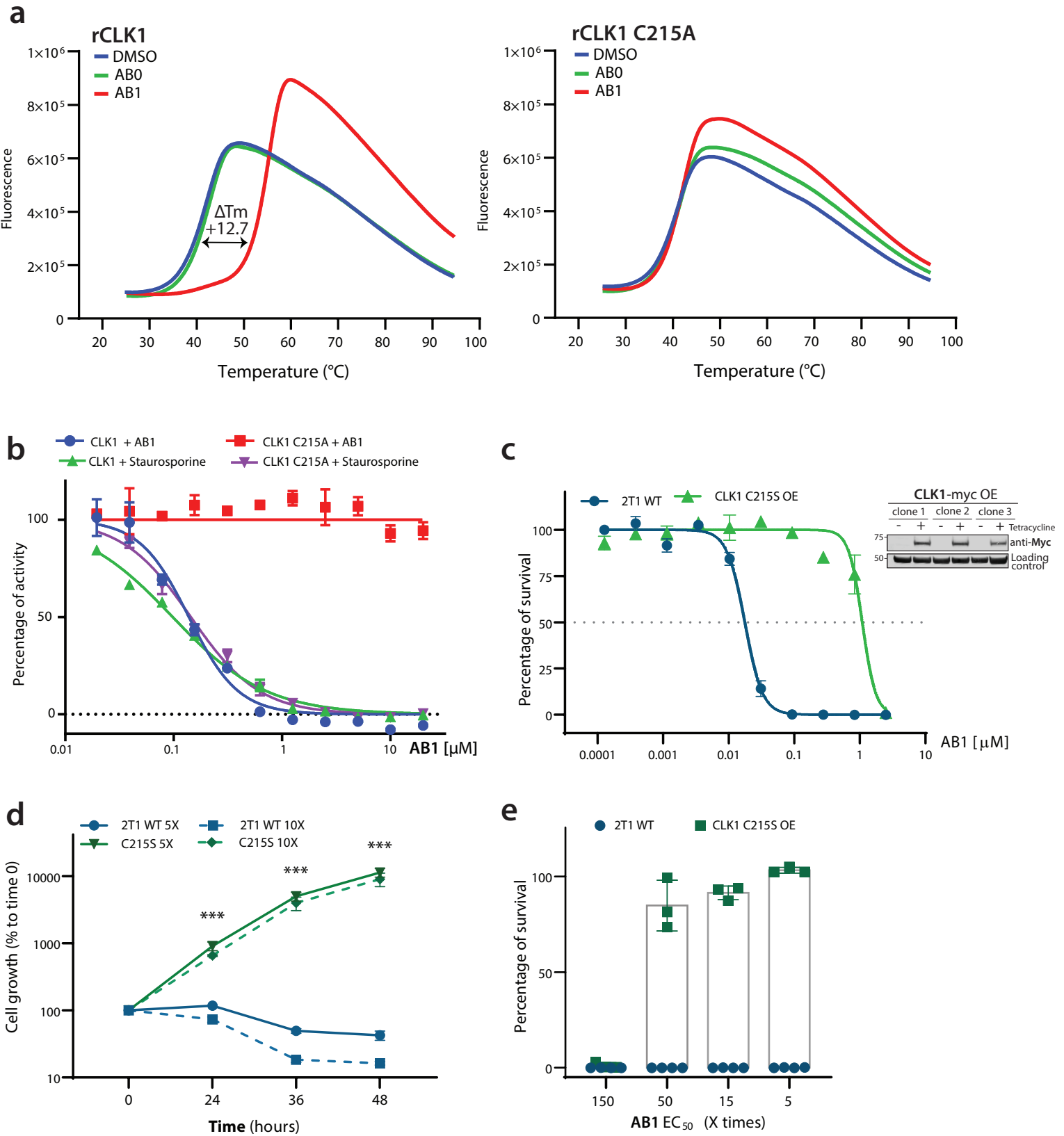
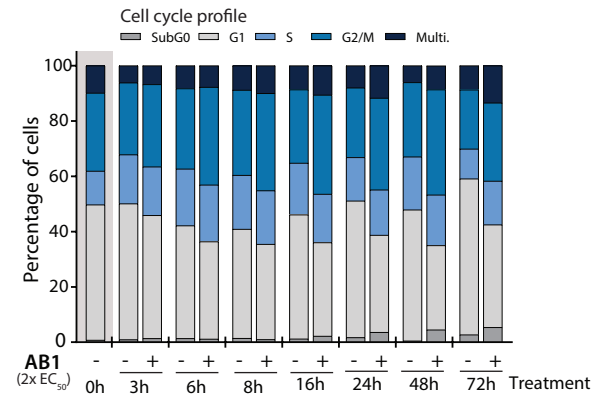
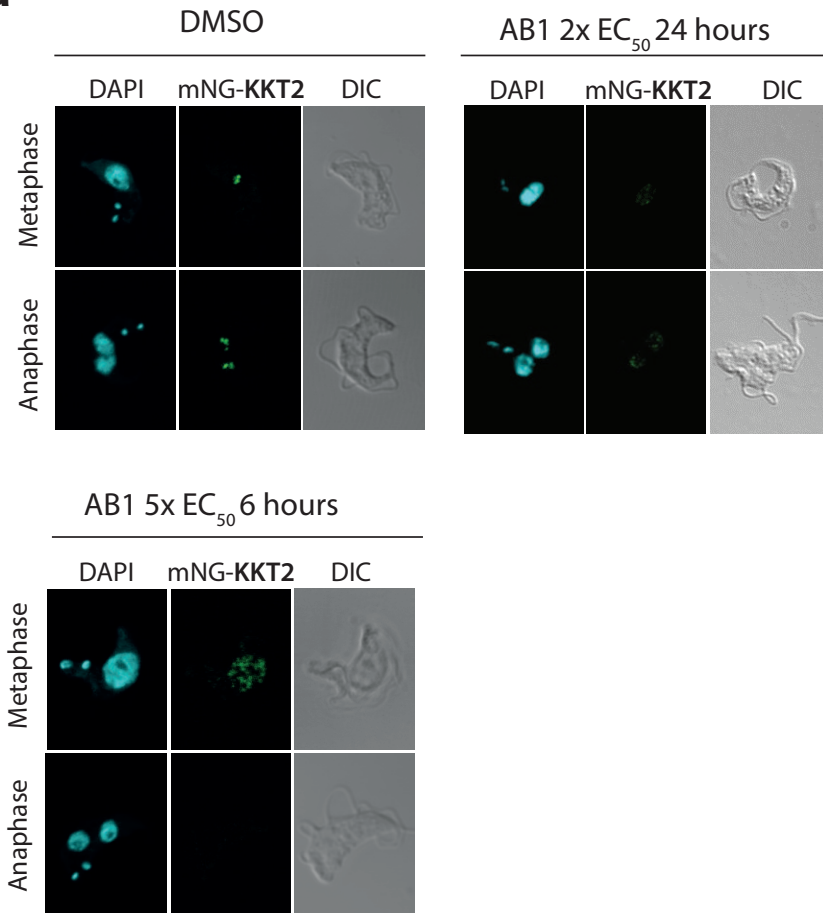


Figure 5

a



b

